Supplementary Material for PCCP

Electronic Supplementary Information for:

Coherent Ultrafast Torsional Motion and Isomerisation of a Biomimetic Dipolar Photoswitch

J. Briand[1], O. Bräm[2], J. Réhault[3], J. Léonard[1], A. Cannizzo[2], M. Chergui[2], V. Zanirato[4], M. Olivucci[5], J. Helbing[3] and S. Haacke[1]

[1] *Institut de Physique et Chimie des Matériaux de Strasbourg, UMR 7504 ULP–CNRS, 67034 Strasbourg (F),*

[2] *Laboratoire de Spectroscopie Ultrarapide, ISIC – EPFL, BSP, CH-1015 Lausanne (CH),*

[3] *Physikalisch-Chemisches Institut,Universität Zürich, Winterthurerstrasse 190, 8057 Zürich, Switzerland*

[4] *Dipartimento di Scienze Farmaceutiche, Università di Ferrara, 44100 Ferrara (I)*

[5] *Dipartimento di Chimica, Università degli Studi di Siena, 53100 Siena (I)*

& Chemistry Dept., Bowling Green State University, Bowling Green, OH 43403 (USA).

Contents

Here we give supplement information regarding the materials and methods (part 1 to 4), as well as a short complement to the discussion, concerning the MeO-NABFP ultrafast dynamics (part 5).

1. Experimental apparatuses and conditions

1.1. Fluorescence up-conversion spectroscopy

The experimental set-up and data processing have been described elsewhere in detail[1-4]. Briefly, the sample is excited at 400 nm at a repetition rate of 100 kHz by ~80-fs, 10-nJ light pulses, focused to a spot of 30 µm (FWHM) diameter in a flow cell. A solution of ZW-NAIP molecules diluted in methanol to an absorbance of 0.7 mm^{-1} at 400 nm is flown in a 0.5-mm thick quartz flow cell at a sufficient speed to avoid photo-degradation and multiple excitations. The fluorescence, collected in forward scattering geometry, is up-converted in a 250-µm-thick beta barium borate (BBO) crystal by mixing it with a gate pulse at 800 nm. A temporal resolution of ca. 120 fs (FWHM) is achieved. The up-converted signal is spatially filtered and detected with a spectrograph and a liquid-N_2 cooled CCD camera in polychromatic mode. Data are recorded from 430 to 690 nm in this experiment, and up to a time delay of 180 ps. The collected fluorescence signal is corrected for the Group Velocity Dispersion (GVD) over the entire detection range.

1.2. UV-Vis transient absorption spectroscopy

The experimental pump/probe setup is based on a Ti:Sapphire regenerative amplifier laser system (Pulsar, Amplitude Technology), delivering 800-nm, 40-fs pulses at a repetition rate of 5 kHz. A pump beam at 400 nm is generated by Second Harmonic Generation (SHG) in a 0.2-mm thick BBO crystal. The probe beam is a white-light continuum (290-950 nm) generated with 800-nm pulses in a 2-mm-thick CaF2 crystal, oscillating orthogonally to the input beam. The pump and probe beams are focused into a 0.5-mm-path- length quartz capillary to a spot diameter of ~120 and ~70 µm, respectively. Their relative polarization is set to magic angle (54.7°). The concentration of the ZW-NAIP/methanol solution is adjusted to an absorbance of 0.7 mm^{-1} at 400 nm. The sample is circulated through the capillary using a peristaltic pump, so as to refresh the excitation volume between two successive pump pulses. The Instrument Response Function (IRF) is approximated by a Gaussian function of ~80 fs FWHM, from the measured temporal width of the stimulated Raman signal of methanol. The excitation energy density is set in the linear regime i.e. below 1mJ/cm^2 per pump pulse. The sample container of 10 mL is carefully kept in the dark throughout the experiment. Probe and reference spectra are recorded using a spectrograph (H25 monochomator, Jobin-Yvon) and a CCD camera (SPEC-10:400B, Princeton Instrument) at a 227-Hz acquisition rate. Data are recorded from 290 to 720 nm in this experiment, with 2.5-nm resolution, and up to a time delay of 100 ps.

1.3. Mid-IR transient absorption spectroscopy

Femtosecond mid-IR probe pulses were detected together with a reference beam by a 32 pixels double array HgCdTe detector with 4 cm^{-1} resolution. Data in three overlapping spectral windows were recorded consecutively under identical conditions and assembled to produce transient spectra between 1475-1675 cm^{-1}. A λ/2 plate in the 390 nm pump beam (<0.5 μJ/pulse, focal spot 150 μm) was rotated every 500 laser shots for the quasi-simultaneous recording of transient spectra with parallel and perpendicular polarization of pump- and probe light, from which magic angle and anisotropy data were calculated. The time-resolution of the set-up was determined by measuring the pump-induced change in mid-IR-transmission of a germanium plate placed at the position of the sample, which yielded a step function with a rise-time of 150 fs (FWHM of the signal derivative). The Kerr signal of the sample cell windows yielded a similar time resolution.

2. ZW-NAIP preparation and UV-VIS steady-state characterization

The zwitterion molecule ZW-NAIP synthetic procedures are described in details elsewhere[5] and the resulting sample powder is diluted in spectroscopy grade methanol. The absorption spectra of the pure E- and Z-isomer have been determined using HPLC[5] and are plotted in figure S-1(A). They are quite similar with absorption peaking at $\lambda_{max}(E)$ = 391 nm and $\lambda_{max}(Z)$ = 397 nm. The E-Z difference spectrum is shown in figure S-1(B) with a maximum at 379 nm and a minimum at 432 nm. NMR spectroscopy indicates that more than 94 % of the molecules are in the Z-isomer form[6] in the dark at room temperature.

Absorption spectra are recorded using a UV-Vis spectrometer (U-3000 spectrophotometer, Hitachi) before and a few minutes after transient absorption experiments and are displayed in figure S-1(C). We observe no sign of sample degradation but rather a Z→E photoconversion as shown by the difference spectrum plotted in figure S-1(D), which overlays very well with the E-Z difference spectrum obtained independently[5] (Figure S-1(B)). This demonstrates the stability of both isomers under the exposure to laser light excitation over the duration of the TA experiments (4-5 hours). The mixture of both isomers evolves from [94% Z ; 6% E] before the TA experiment to [85% Z ; 15% E] after. The E isomer contribution to the signal is thus ~10 % in average over the experiment duration.

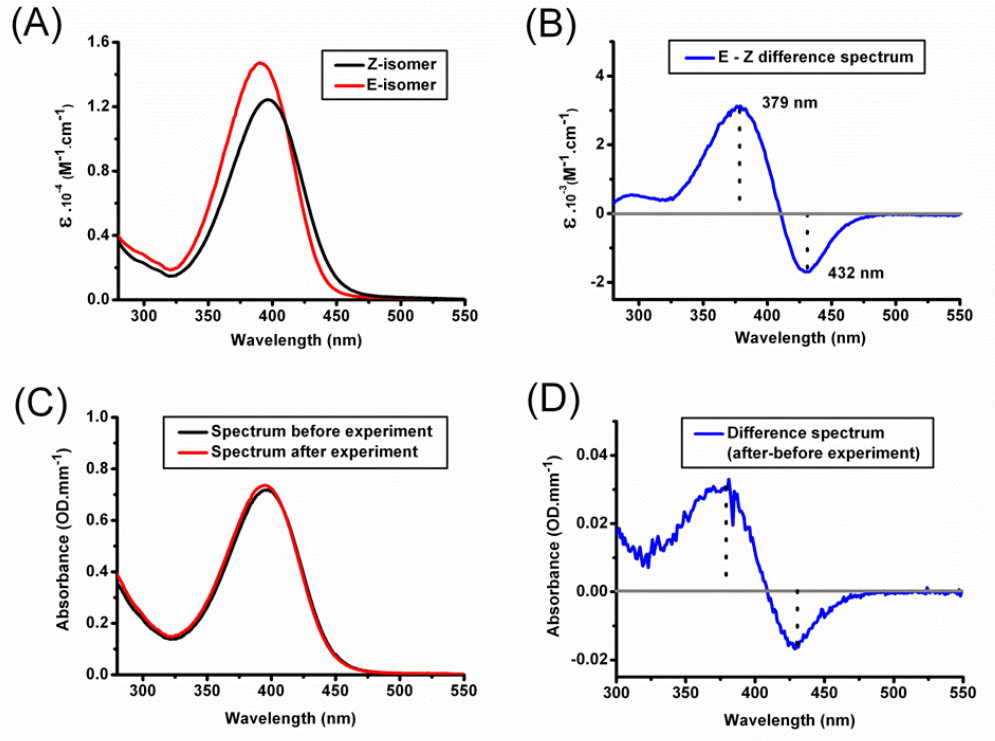

Figure S-1. **(A)** Absorption spectra of pure E- and Z-isomers (Data from L. Latterini et al[5]**). (B)** E-Z difference spectra with a maximum at 379 nm and a minimum at 432 nm. **(C)** Sample absorption spectra measured before and after transient absorption experiments and **(D)** their difference showing weak E to Z photoconversion.

3. Femtosecond mid-IR experiments

3.1. Calculated vibrational spectra used for mode identification

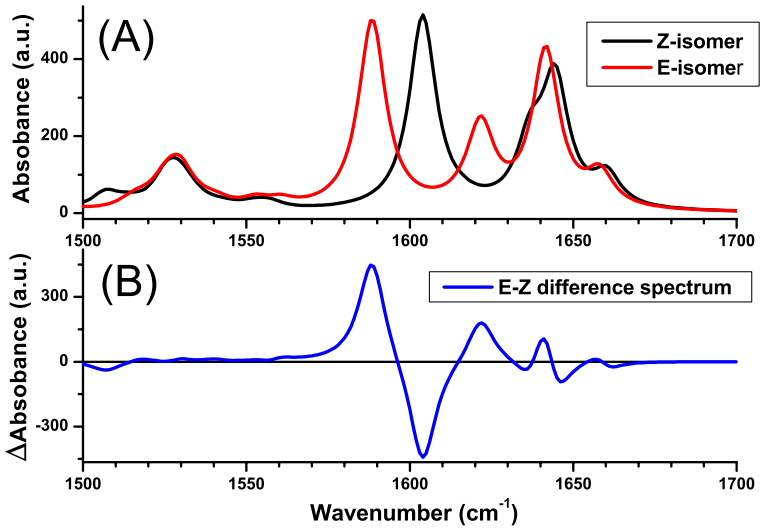

Figure S-2. Harmonic normal mode spectra of Z and E forms of the ZW-NAIP switch in the gas phase (B3LPY, 6-31G+ basis set). The mode at 1605 (1586 for E) is dominated by in phase C1'-C4 and C=N stretch motion, the two modes near 1640 cm^{-1} (1620 and 1640 cm^{-1} for E) are characterized by asymmetric C=O stretch motion. The band near 1660 cm^{-1} involves the deformation of the 6-membered ring of the indanylidene moiety. Note that we can make only a qualitative comparison between experiment and calculations. For example, in the gas phase optimized structure the carboxylate group is rotated with respect to the QM/MM solution structure reported in ref. [5,7].

3.2. Concentration dependence

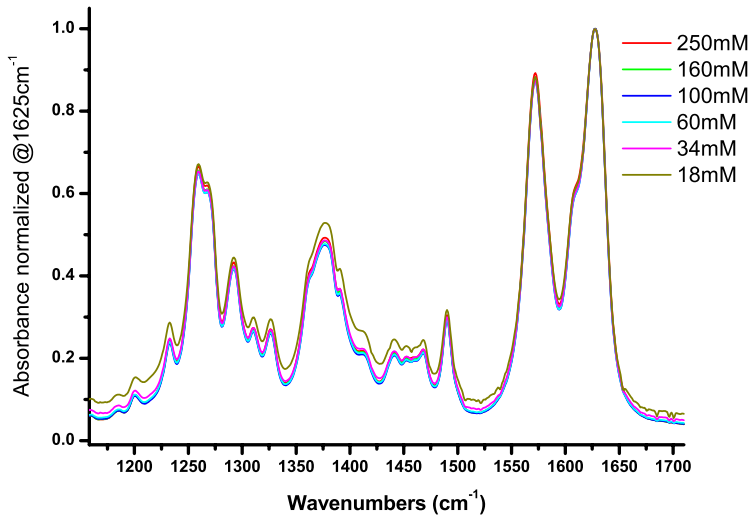

Figure S-3. Normalized FTIR spectra of ZW-NAIP at different concentrations. No signs of aggregation are visible up to concentrations far beyond the concentration (20 mM) used in the transient experiments.

3.3. Time resolution

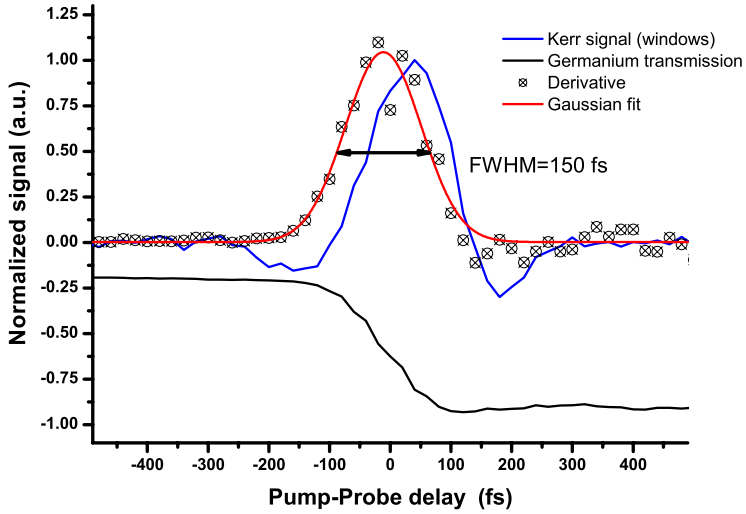

Figure S-4. The pump-induced mid-IR transmission change of a germanium plate (placed behind a CaF_2 window at the position of the sample) is a step function (solid black line), whose derivative (squares) yields a time-resolution of 150 fs (Gaussian fit, red line). Pulse overlap and Kerr signal (blue line, signal at 1600 cm^{-1}) are negligable after 300 fs.

3.4. Background subtraction

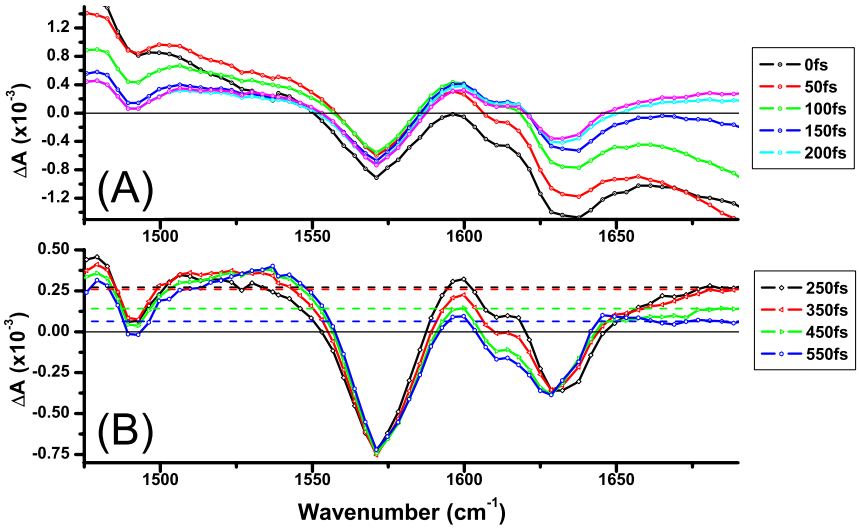

Figure S-5. Uncorrected mid-IR pump-probe data for Z-excitation. Up to delays of 250 fs (grey lines), pulse overlap leads to strong cross phase modulation and perturbed free induction decay signals,

which cannot be unambiguously subtracted from the data. Between 250 fs and 500 fs a constant background, given by the signal at 1690 cm^{-1} (horizontal lines) was subtracted.

4. Transient UV-VIS absorption data processing

Concerning the fluorescence up-conversion setup, experimental settings and group velocity dispersion (GVD) correction have been described elsewhere in detail[1-4].

In the UV-Vis transient absorption experiment, the combined response of pure solvent and quartz capillary is always measured, in the same experimental conditions as for the ZW-NAIP sample. This ultrafast response called "solvent response" hereafter is mostly composed of cross-phase modulation (XPM), two-photon absorption (TPA) and stimulated Raman amplification (SRA)[8-10]. It overlaps with the early time signature of ZW-NAIP. Therefore, the quantitative analysis of the rise and decay of the ZW-NAIP excited state contributions can only be carried out after subtraction of the solvent response[9]. However, we also use the solvent response to determine the GVD, and thus to correct for it over the entire measured wavelength range (300-700 nm).

4.1. Group velocity dispersion (GVD) compensation

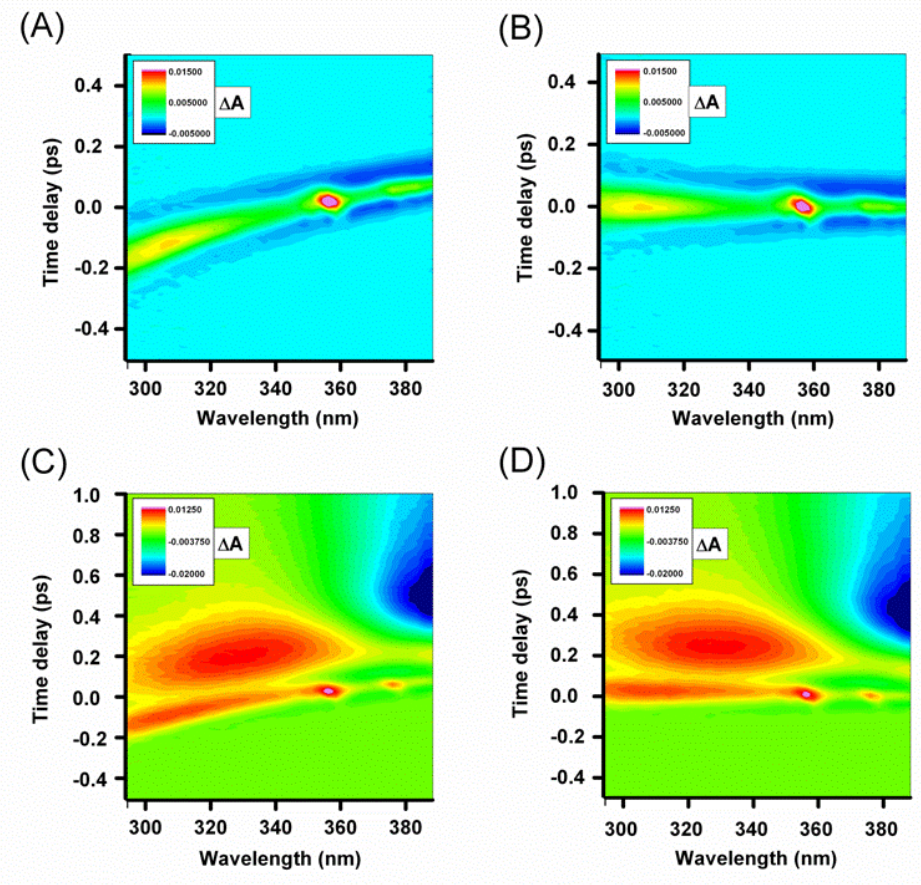

Figure S-6. (A) Raw transient UV absorption data of MeOH in the quartz capillary for time delays between -0.5 and 0.5 ps. **(B)** Same as A after GVD compensation. **(C)** Raw transient absorption data

of ZW-NAIP in MeOH in the -0.5 to 1 ps time range. **(D)**. Same as C after GVD compensation. In figure C and D, the solvent signal overlaps with the ESA and GSB of ZW-NAIP.

At each individual probe wavelength, time zero is defined within ± 10 fs as being the time-axis mid-point of the coherent solvent signal in agreement with XPM simulations[9]. In order to compensate for the GVD, a third order polynome is used to fit the location of the wavelength-dependent time zero and the time axis is shifted accordingly. Figures S-6 shows the signal of the pure solvent and ZW-NAIP in solution before and after the GVD correction in the UV region, where the chirp is most pronounced. The same procedure is applied to data measured in the Vis spectral range (see figure S-7(B)).

4.2. Solvent response subtraction

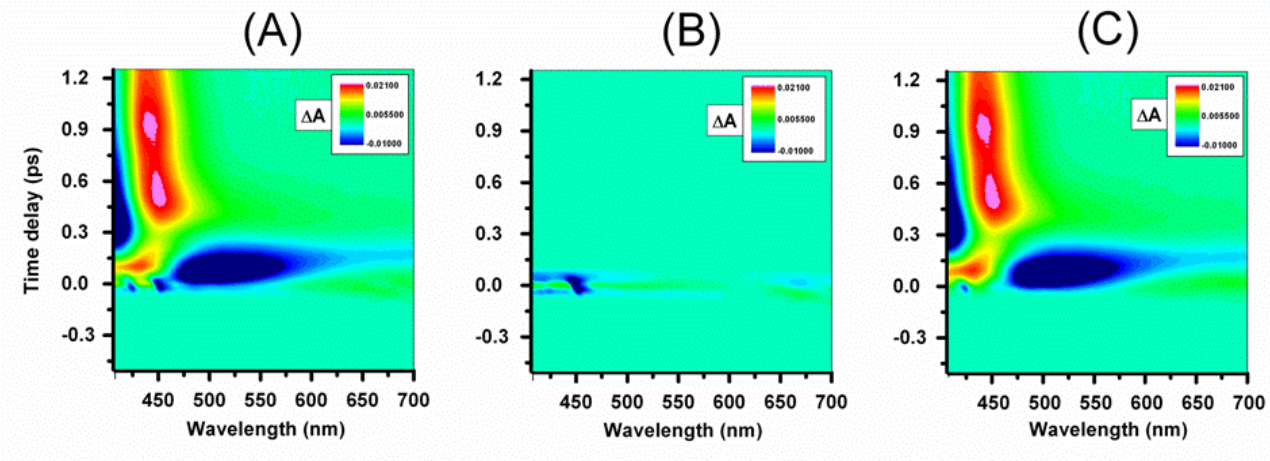

Figure S-7. Time-resolved visible transient absorption change ΔA of **(A)** ZW-NAIP and **(B)** pure solvent measured separately under the same experimental conditions. Positive ΔA is coded in red and negative in blue **(C)** Result of the subtraction of the solvent signal (B) from the raw data (A). Note that the color scale is the same in the three graphs.

Figure S-7(C) presents the result of the subtraction of the solvent data (fig. S-7(B)) from the raw data (fig. S-7(A)). A multiplication factor (<1) is used to take into account the ZW-NAIP absorption at the excitation wavelength. Figure S-8 illustrates at four selected wavelengths how efficiently the solvent signal is removed by this procedure.

The solvent signal contains strong methanol SRA (Stokes and anti-Stokes) signals at ~450 nm (see fig S-7(B)) and ~357 nm (fig. S-6(D)), which are used for determining the temporal resolution of the experiment: a fit to a Gaussian function reveals an 80-fs FWHM Instrument Response Function (IRF). After solvent signal subtraction, SRA signals remain at ~425 nm (fig.S7-(C)) and ~376 nm (fig. S6-(D)). They are ~1600 ± 100 cm^{-1} blue- and red-shifted from the excitation wavelength, and can thus be

assigned to C=C, C=N or C=O stretching modes of the ZW-NAIP molecule in agreement with the mid-IR data.

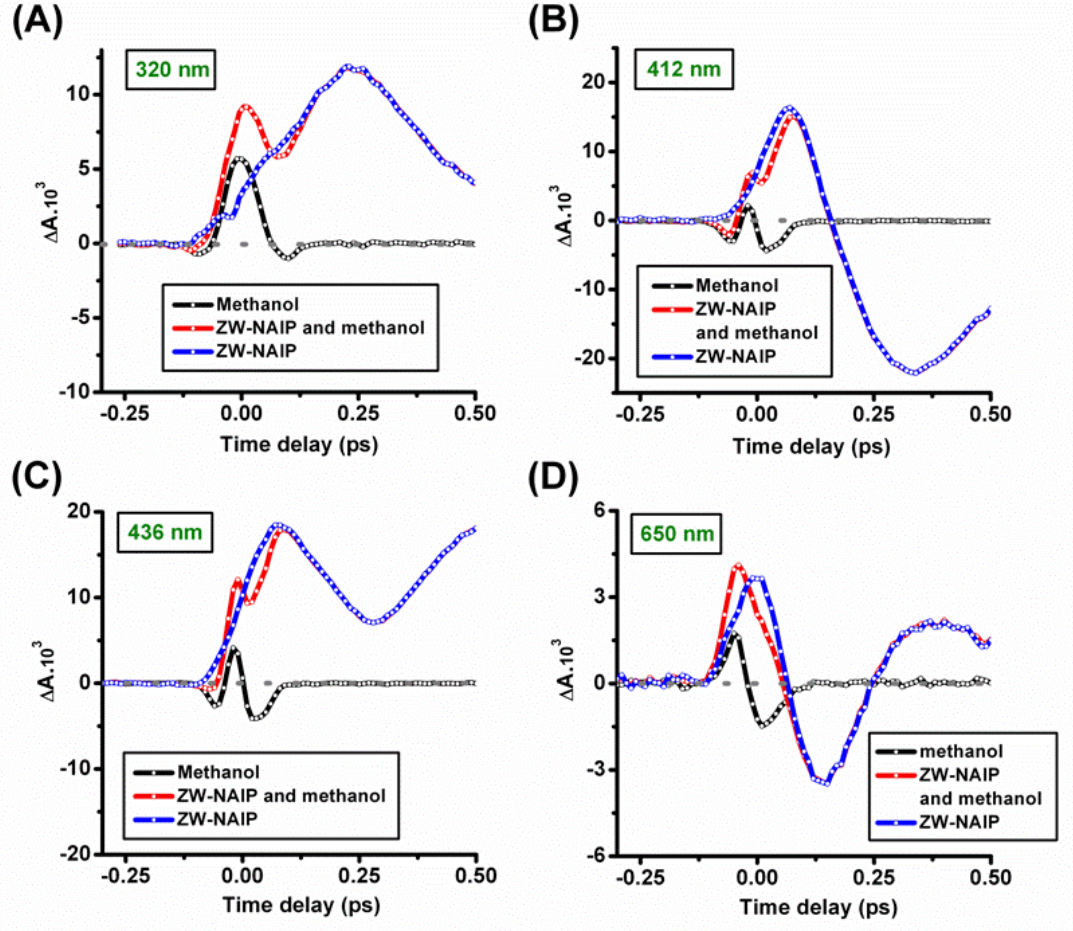

Figure S-8. Kinetic traces of ZW-NAIP (blue curve) obtained after subtraction of the solvent response (black curve), from the raw data (red curve) at **(A)** 320 nm, **(B)** 412 nm,**(C)** 436 nm and **(D)** 650 nm.

5. Fluorescence and transient absorption data analysis

5.1. Fluorescence up-conversion data analysis

The fluorescence up-conversion signals are analysed using a function S(t) defined as the sum of decaying exponential functions multiplied by the Heavyside step function H(t-t_0) centered on the signal onset time t_0 and convoluted with the instrument response function (IRF) of the system, assumed to be Gaussian:

$$S(t) = \left\{ H(t-t_0) \times \sum_i A_i e^{-\frac{t-t_0}{\tau_i}} \right\} \otimes e^{-0.5\left(\frac{t}{\sigma}\right)^2} \qquad (1)$$

In figure 3B of the manuscript the kinetic trace at 502 nm is fitted by this function S(t). A Singular Value Decomposition (SVD) is also applied on the whole fluorescence dataset. Figure S-9(A) show the resulting singular values (SV). As shown in Figure S-9(B) the fluorescence spectrum is essentially given by the first, dominating component whereas the weighted sum of the spectra associated to the 2nd and 3^{d} singular values mainly account for the solvent Raman signal around 450 nm. In addition, reconstructing the signal associated to the fourth and all the weaker components yields a featureless noise matrix (not shown). Thus only the first time vector is used for analysis in this particular case. The fitting to S(t) (figure S8-(C)) yields two exponential decays of 0.14 and 1 ps, and a small offset. Reconstructing the Decay Associated Spectra (DAS) of the two major decays leads to figure 3C in the paper. A cross-check was made by spectrally truncating the dataset (470-680 nm), to avoid the Raman contribution region, and then performing the same analysis, yielding the same results. Another alternative analysis was performed with the first 3 SVs and yielded the same DAS and another one accounting for the Raman contribution.

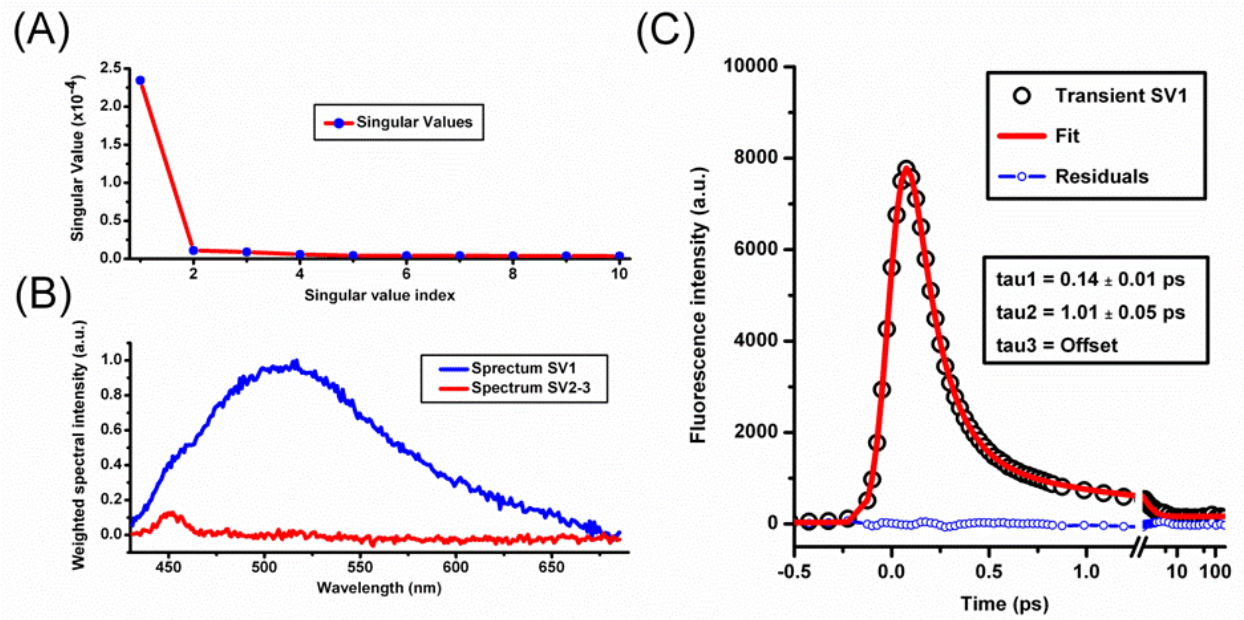

Figure S-9. (A). First ten Singular Values (blue dots) from the data decomposition. **(B)**. Spectral intensity of SV1 (blue line) and the weighted sum of SV2 and SV3 (red line) associated spectra. **(C)**. Fit (red line) of the first time vector (black circles) using 2 exponential decays and a small offset, and the corresponding residuals (blue line and dots).

5.2. UV-Vis transient absorption data analysis

5.2.1. SVD and global analysis

As there are dynamically shifting bands and oscillations in the early times of the TA data, we have performed SVD and global analysis only at time delays > 1.2 ps, where these features are negligible. Doing so, we obtain the ground state (GS) relaxation signals. The fitting function S(t) given by eq. (1) was used with the time origin t_0 set to 300 fs, as the GS signals only start to decay after this time shift. The fitting of the 4 most prominent SVD time vectors is shown in figure S-10(A). The dominant time constants are 1.09 ± 0.02 ps and 4.85 ± 0.03 ps, and an infinite time constant (offset function). The resulting DADS are shown in figure 7 of the paper. The infinite-time DADS overlays almost perfectly with the spectrum referred to as the quasi-static spectrum in the manuscript. A very weak ($\Delta A = 2.10^{-4}$) and spectrally unstructured component of 78.5 ± 15 ps is needed for better fitting. It is most probably due to imperfect magic angle conditions and is thus neglected in the data analysis and discussion.

The same type of analysis is performed on the 300-330 nm spectral range of the TA data (fig. S-10(B)) for time delays > 0.35 ps. In this spectral range, the ground state bleach is minimum and the ESA is observed almost pure. The analysis reveals a dominant (~90%) component of 0.15 ps assigned to the

residence time of the wave packet in the observation spectral range. A slower and weaker component of 0.85 ps (~10%) is found similarly as in the fluorescence analysis and the TA global analysis (t>1.2 ps) presented above. A longer, weak and also positive component of several ps is needed for better fitting and probably corresponds to a hot ground state signal from the S_0-S_2 transition (290 nm).

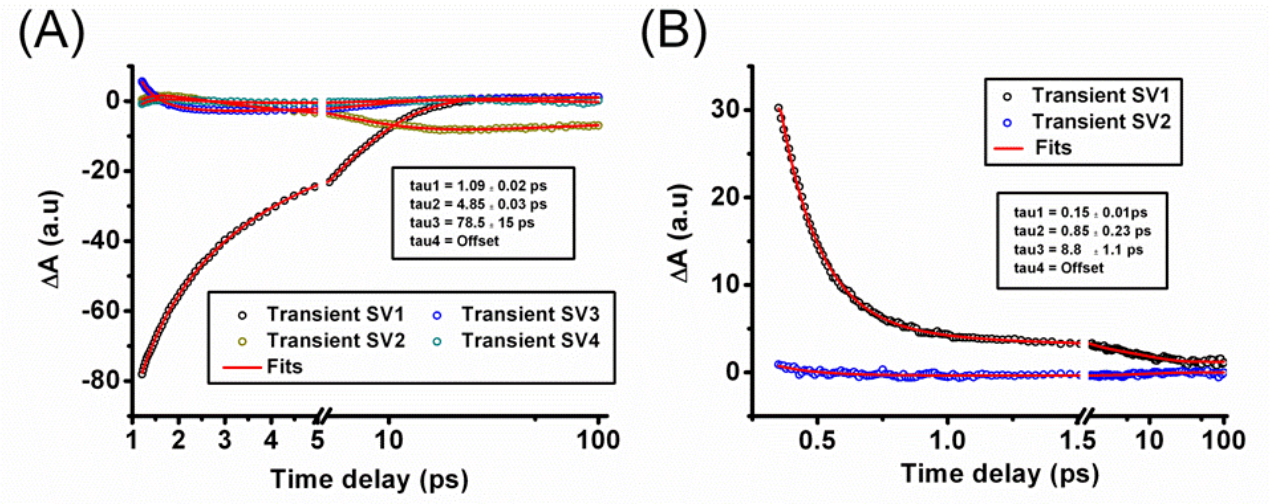

Figure S-10. (A). Global fitting of the four prominent time vectors (black, gold, blue and cyan circles, respectively) for the full transient absorption spectral dataset analysed at time delays > 1.2 ps, and their corresponding fits (red lines). **(B)**. Global fitting of the two prominent time vectors (First (second) time vector in black (blue) circles, corresponding fit in red line) resulting from the SVD of the 300-330 nm region for time delays > 0.35 ps.

5.2.2. Justification of the fitting model

In the case of UV-Vis transient absorption, using only exponential functions as defined in equation (1), leads to unsatisfactory results for early time dynamics (<1.2 ps). As clearly shown at 510 nm in figure S-11(A), a sum of IRF-limited exponential rise and decay is unable to fit the peak-like character of the data at early times. Moreover, fitting with exponential functions yields unrealistically large amplitudes for example at wavelength around 650 nm (see figure S-11(C)) with a maximum amplitude of -0.115 for the SE contribution. This is about 10 times larger than what is expected at this wavelength assuming equal oscillator strength for absorption and emission. Figure S-11(D) (at 320 nm) shows a simulation including the same decay time constants as given in the paper but including a convolution with a fixed 80-fs IRF value. This unambiguously shows the need for a larger Gaussian standard deviation value as well as a time-shift, reflecting the wave packet time-spreading and shifting as the reaction proceeds.

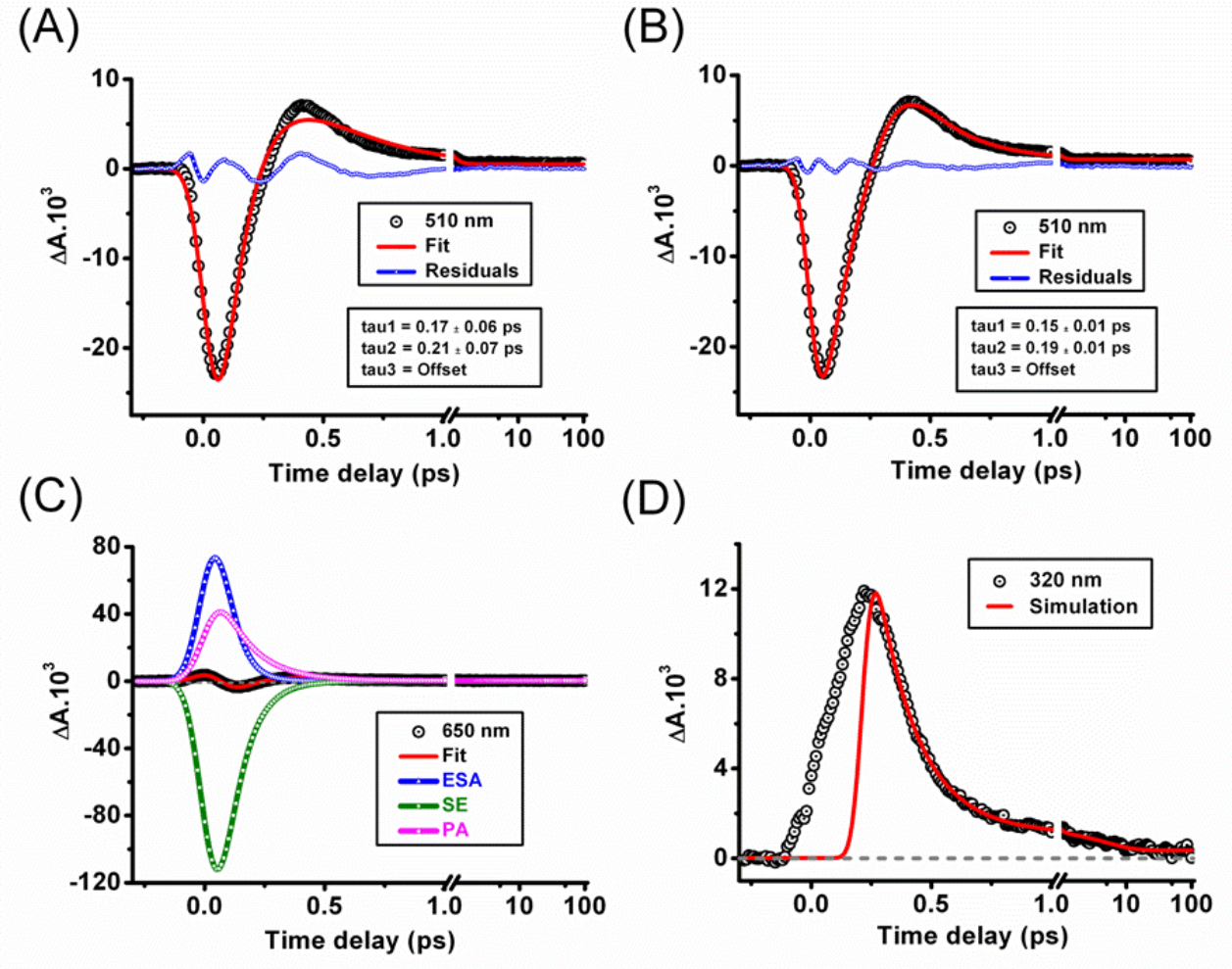

Figure S-11. Kinetic trace (black circles), fit (red line) and residuals (blue line) at 510 nm using **(A)** eq. (1) and **(B)** the delayed exponential function given by Eq. 6 for the PA contribution. A significant improvement of the fit is obtained is case (B) **(C)**. Kinetic trace at 650 nm (black circles) and fit (red line) using Eq. (1) as a fitting function. With this fit, the different contributions to the signal show unrealistic amplitudes. **(D)**. Kinetic trace at 320 nm (black circles) together with a simulation (red line) using the IRF for the convolution.

To overcome the difficulties mentioned above, the fitting functions used for the data analysis of specific kinetic traces are those given below (Eq. 2 to 7) rather than Eq. 1. Each function is associated with a specific transition discussed in the paper. When kinetic traces are fitted, the different functions corresponding to the signals (SE, ESA1-2-3, GSB and PA, see eq. (2)-(7)) present at this specific wavelength are included. A Gaussian standard deviation (σ) larger than the IRF is found for the ESA3 and PA signals along with a time-shift with respect to t_0. Alternative fits were tried, using for example a delayed exponential rise instead of a delayed and larger Gaussian standard deviation for the PA, and the results were very similar.

According to a wave packet-like PA formation, the bleach does not recover during a period t_{GSB}, as implemented by the argument shift in the Heavyside function $H(t-t_0-t_{GSB})$. Eq. (7) thus models a constant bleach signal A_{GSB} before t_{GSB}, the latter being a fit parameter.

$$SE(t) = \left\{ H(t-t_0) \times A_{SE}\, e^{-\frac{t-t_0}{\tau_{SE}}} \right\} \otimes e^{-0.5\left(\frac{t}{\sigma}\right)^2} \qquad (2)$$

$$ESA1(t) = \left\{ H(t-t_0) \times A_{ESA1}\, e^{-\frac{t-t_0}{\tau_{ESA1}}} \right\} \otimes e^{-0.5\left(\frac{t}{\sigma}\right)^2} \qquad (3)$$

$$ESA2(t) = \left\{ H(t-t_0) \times A_{ESA2}\, e^{-\frac{t-t_0}{\tau_{ESA2}}} \right\} \otimes e^{-0.5\left(\frac{t}{\sigma}\right)^2} \qquad (4)$$

$$ESA3(t) = \left\{ H(t-t_0-t_{ESA3}) \times \sum_i A_{ESA3_i}\, e^{-\frac{t-t_0-t_{ESA3}}{\tau_{ESA3_i}}} \right\} \otimes e^{-0.5\left(\frac{t}{\sigma_{ESA3}}\right)^2} \qquad (5)$$

$$PA(t) = \left\{ H(t-t_0-t_{PA}) \times \sum_i A_{PA_i}\, e^{-\frac{t-t_0-t_{PA}}{\tau_{PA_i}}} \right\} \otimes e^{-0.5\left(\frac{t}{\sigma_{PA}}\right)^2} \qquad (6)$$

$$GSB(t) = \left\{ \sum_i A_{GSB\,i} \times \left(H(t-t_0) - \left(H(t-t_0-t_{GSB}) \times (1 - e^{-\frac{t-t_0-t_{GSB}}{\tau_{GSB_i}}}) \right) \right) \right\} \otimes e^{-0.5\left(\frac{t}{\sigma}\right)^2} \qquad (7)$$

As these fits are performed at individual wavelengths, some parameters are λ-dependent, representing the wave packet behaviour. In particular, the PA onset time t_{PA} shifts from 240 to 300 fs as wavelength is varied from 650 to 410 nm, as a result of this fitting procedure.

	ESA	SE	GSB	PA
650 nm	A_{ESA1} = 0.041 τ_{ESA1} = 0.05 ps	A_{SE} = -0.018 τ_{SE} = 0.15 ps	---	t_{PA} = 240 fs, σ_{PA} = 175 fs A_{PA1} = 7.10^{-3}, τ_{PA1} = 0.19 ps A_{PA2} = 4.10^{-4}, τ_{PA2} = Offset
509 nm	---	A_{SE} = -0.039 τ_{SE} = 0.15 ps	---	t_{PA} = 260 fs, σ_{PA} = 270 fs A_{PA1} = 0.021, τ_{PA1} = 0.19 ps A_{PA2} = 7.10^{-4}, τ_{PA2} = Offset
410 nm	A_{ESA2} = 0.085 τ_{ESA2} = 0.14 ps	---	t_{GS} = 300 fs A_{GS1} = -0.035, τ_{GS1} = 0.27 ps A_{GS2} = 10^{-3}, τ_{GS2} = 11 ps A_{GS3} = 5.10^{-4}, τ_{GS3} = Offset	
320 nm	t_{ESA3} = 130 fs, σ_{ESA3} = 280 fs $A_{ESA3(1)}$ = 0.031 $\tau_{ESA3(1)}$ = 0.13 ps $A_{ESA3(2)}$ = 10^{-3} $\tau_{ESA3(2)}$ = 2.7 ps	---	---	---

Table S-1. Table summarizing the fitting parameter values from the four different fits at 650, 509, 410 and 320 nm presented Figure 6 of the paper. For each fit, t_0 is ~0 ps and $\sigma = \sigma_{IRF}$ = ~80fs, unless other value is specified.

5.2.3. Oscillations analysis

The observed oscillatory signals are analyzed with a delayed exponentially damped sine function *Oscill(t)*, added to the above PA(t) and GSB(t) functions used to describe incoherent relaxation. Hence, the fitting function writes $F(t) = PA(t) + GSB(t) + Oscill(t)$ with:

$$Oscill(t) = H(t - t_0 - t_{start}) \times A_{osc} \times \cos\left(2\pi\left(\frac{t - t_0 - t_{start}}{T_{osc}}\right) + \Phi_{osc}\right) \times e^{-\frac{t - t_0 - t_{start}}{\tau_{dec}}} \quad (8),$$

where $\mathbf{A_{osc}}$ is the amplitude, $\mathbf{T_{osc}}$ the period and $\mathbf{\Phi_{osc}}$ the phase of the oscillations. $\mathbf{\tau_{dec}}$ is the decoherence (dephasing) decay time. A time-shift $\mathbf{t_{start}}$ is used to account for the fact that oscillations start only after a time delay with respect to t_0.

A simultaneous fit of a blue-sided (368nm) and a red-sided (446 nm) absorption wavelength is done, using the same decay times for the incoherent part $PA(t) + GSB(t)$, and the same oscillation period and decoherence time, at both wavelengths. The kinetic traces and their corresponding fits are presented in figure S-12(A) together with the residuals. Figure S-12(B) separates the incoherent contribution from the oscillatory part by subtracting $PA(t) + GSB(t)$ obtained with the fitting procedure from the raw

kinetic traces for both wavelengths. The oscillatory residuals are presented in figure S-12(C), together with the corresponding *Oscill(t)* resulting from the fit of the raw data by F(t).

The decay constants obtained here for the incoherent part are in good agreement with the SVD analysis. The oscillatory part has a period $\mathbf{T_{osc}}$ = 560 ± 10 fs and a dephasing time $\boldsymbol{\tau_{dec}}$ = 320 ± 20 fs.

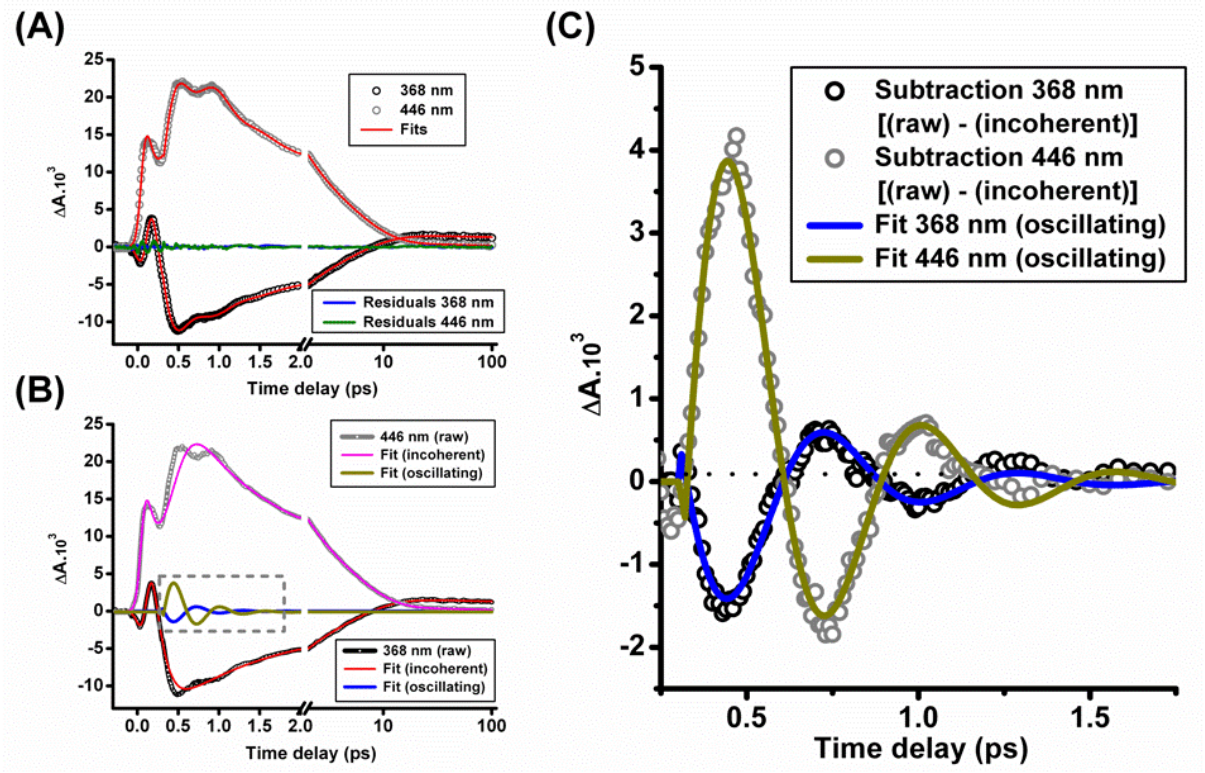

Figure S-12. **(A)**. Kinetic trace (black (gray) open circles) together with its corresponding fit (red lines) and residuals (blue (green) line) at 368 nm (446 nm). **(B)**. Kinetic traces at 368 and 446 nm together with the two parts (incoherent and oscillating, see text for details) of each fitting function. **(C)**. Oscillatory residuals and fits.

6. Dynamics of the MeO-NABFP molecule

In order to prove the fact that a Resonant Impulsive Raman Scattering (RIRS) process is not responsible for the observed oscillatory features, we present other data measured in the same experimental conditions as the ones described above on a structurally very similar molecule. The molecule is MeO-NABFP (methoxy N-alkylated benzofurano pyrroline). Its absorption spectrum and structure are shown in Figure S-13(A). When compared with the previously studied MeO-NAIP[11], MeO-NABFP differs only by one oxygen atom replacing a carbon atom on the indanylidene moiety and causing a red-shift of its absorption spectrum by ~30 nm (λ_{max} = 429 nm).

MeO-NABFP signals do not show any delayed PA or oscillatory features at any wavelength. Its isomerization dynamics can be described by exponentially decaying functions such as Eq.1, with a 650-fs decay of the SE and ESA signals. We argue that if the oscillatory features were due to RIRS in

MeO-NAIP and ZW-NAIP, they should be also present in the structurally almost identical MeO-NABFP molecule. As shown in Figure S-13(B), no oscillations are observed in the kinetic traces on the blue and red sides of the S_0-S_1 absorption band of MeO-NABFP.

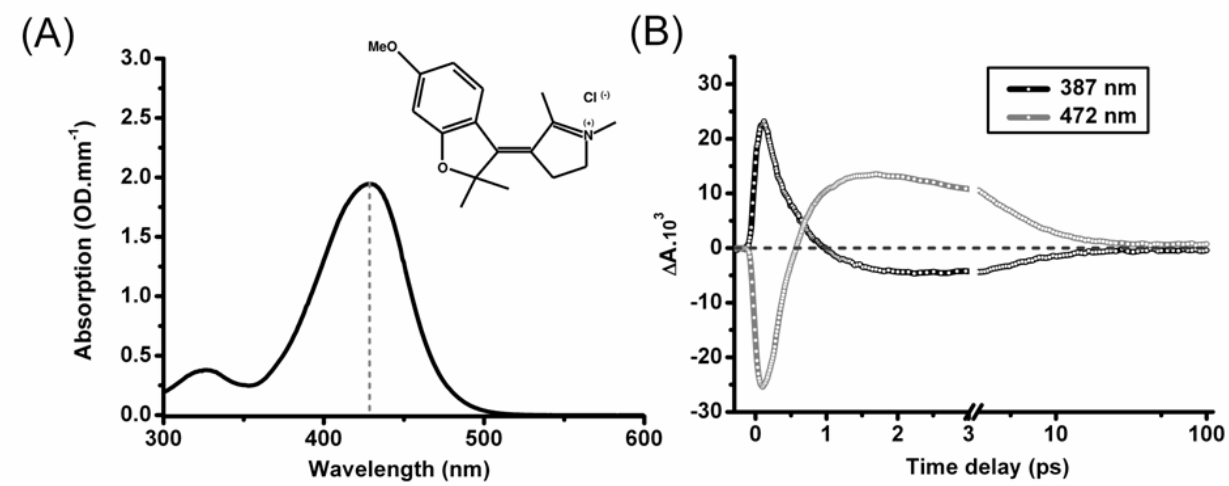

Figure S-13. **(A)**. Absorption spectrum of the MeO-NABFP molecule (λ_{max} = 429 nm) together with its structure. **(B)**. Kinetic traces on the blue (387 nm) and red (472 nm) sides of the absorption spectrum. No oscillations are seen in the data.

References:

(1) Cannizzo, A.; Bräm, O.; Zgrablić, G.; Tortschanoff, A.; Oskouei, A. A.; van Mourik, F.; Chergui, M. *Opt. Lett.* **2007**, *32*, 3555.

(2) Zgrablić, G.; Haacke, S.; Chergui, M. *Chemical Physics* **2007**, *338*, 168.

(3) Zgrablić, G., Ecole Polytechnique Fédérale de Lausanne, 2006.

(4) Zgrablić, G.; Voïtchovsky, K.; Kindermann, M.; Haacke, S.; Chergui, M. *Biophysical Journal* **2005**, *88*, 2779.

(5) Melloni, A.; Paccani, R. R.; Donati, D.; Zanirato, V.; Sinicropi, A.; Parisi, M. L.; Martin, E.; Basosi, R.; Fusi, S.; Latterini, L.; Ferré, N.; Olivucci, M. *submitted* **2009**.

(6) Réhault, J.; Zanirato, V.; Helbing, J.; Olivucci, M. *to be published*.

(7) Sinicropi, A.; Martin, E.; Ryazantsev, M.; Helbing, J.; Briand, J.; Sharma, D.; Léonard, J.; Haacke, S.; Cannizzo, A.; Chergui, M.; Zanirato, V.; Fusi, S.; Santoro, F.; Basosi, R.; Ferré, N.; Olivucci, M. *Proc. Nat. Acad. Sc. USA* **2008**, *105*, 17642-17647.

(8) Lorenc, M.; Ziolek, M.; Naskrecki, R.; Karolczak, J.; Kubicki, J.; Maciejewski, A. *Applied Physics B: Lasers and Optics* **2002**, *74*, 19.

(9) Kovalenko, S. A.; Dobryakov, A. L.; Ruthmann, J.; Ernsting, N. P. *Physical Review A* **1999**, *59*, 2369.

(10) Kovalenko, S. A.; Ruthmann, J.; Ernsting, N. P. *The Journal of Chemical Physics* **1998**, *109*, 1894.

(11) Sinicropi, A.; Martin, E.; Ryazantsev, M.; Helbing, J.; Briand, J.; Sharma, D.; Léonard, J.; Haacke, S.; Cannizzo, A.; Chergui, M.; Zanirato, V.; Fusi, S.; Santoro, F.; Basosi, R.; Ferré, N.; Olivucci, M. *Proceedings of the National Academy of Sciences* **2008**, *105*, 17642-17647.